

University of Reading
Department of Computer Science

Generating Tree Species Classification and Change Maps to Assist Mitigate Climate Change

Pedro Junio

Supervisor: Muhammad Shahzad

A report submitted in partial fulfillment of the requirements of
the University of Reading for the degree of
Master of Science in *Data Science and Advanced Computing*

August 21, 2024

Declaration

I, Pedro Junio, of the Department of Computer Science, University of Reading, confirm that this is my own work and figures, tables, equations, code snippets, artworks, and illustrations in this report are original and have not been taken from any other person's work, except where the works of others have been explicitly acknowledged, quoted, and referenced. I understand that if failing to do so will be considered a case of plagiarism. Plagiarism is a form of academic misconduct and will be penalized accordingly.

I give consent to a copy of my report being shared with future students as an exemplar.

I give consent for my work to be made available more widely to members of UoR and public with interest in teaching, learning, and research.

Pedro Junio
August 21, 2024

Abstract

TODO update at the end

Variety of tree species are crucial in reducing the vulnerabilities and offering stable ecosystem functioning. The precise quantification and assessment of existing tree species on global-scale is therefore essential in filling the science-policy gaps by providing key insights essential in promoting the success of natural climate solutions and devising effective climate mitigation policies. To this end, this study aims to develop novel deep learning based algorithms by using the multi-temporal multi-spectral imagery to generate large-scale forest/tree species classification maps.

Keywords: Convolutional Neural Network, Sentinel-2, Copernicus, SoilGrid, EU-Forest, Forests, Tree Genera, Climate

Report's total word count: over 9000

Contents

1	Data Exploration	1
1.1	EU-Forest Labels	1
1.2	Sentinel-2 Features	3
1.3	Copernicus DEM GLO-30	7
1.4	SoilGrids	8
2	Feature Selection	10
2.1	Sentinel-2 Seasons	10
2.2	Sentinel-2 Bands	11
2.3	Soil and Elevation	13
3	Neural Network Configuration	14
3.1	Hyperparameter Optimization	14
3.2	Model Architecture	15
4	Climate Analysis	17
4.1	ECMWF Reanalysis v5 Dataset	17

List of Figures

1.1	Map of the most common tree genera in EU-Forest.	1
1.2	Distribution of genera (left) and species (right) in EU-Forest.	2
1.3	Distribution of genera (left) and species (right) per location.	2
1.4	Sentinel-2 mission infographic. It highlights important facts and achievements of the mission. Courtesy of ESA	3
1.5	Multiple sample locations overlaid on Google Earth (left) and Sentinel-2 (right) images.	4
1.6	Sample location overlaid on Google Earth (left) and Sentinel-2 (right) images.	4
1.7	Distributions for surface reflectance (left), including a sample means as a dotted line, and z-score normalization (right) for RGB bands.	5
1.8	Distributions for surface reflectance (left), including a sample means as a dotted line, and z-score normalization (right) for NIR bands.	5
1.9	Distributions for surface reflectance (left), including a sample means as a dotted line, and z-score normalization (right) for SWIR bands.	6
1.10	Seasonal Sentinel-2 band correlations.	7
1.11	Distributions for elevation (left), including a sample means as a dotted line, and z-score normalization (right) for the Copernicus DEM GLO-30 dataset.	8
1.12	Distributions for soil properties (left), including a sample means as a dotted line, and z-score normalization (right) for the SoilGrids dataset.	8
2.1	Seasonal Sentinel-2 analysis for all season combinations using a 3D CNN.	10
2.2	Sentinel-2 analysis for all combinations within three band groups using a CNN. The horizontal black line represents the weighted f1-score for all bands.	12
2.3	Sentinel-2 analysis for selected combinations between each of the three groups using a CNN. The horizontal black line represents the weighted f1-score for all bands.	12
2.4	Analysis of SoilGrids and elevation data integration.	13
3.1	The top f2-scores for the initial hyperparameter tuning process are highlighted, with the best score marked by a diamond shape.	15
3.2	The model's layered architecture is depicted. The top-right shows the input layers, the middle section displays the convolutional layers, and the bottom-right illustrates the fully-connected layers. The layered views were generated using VisualKeras (Gavrikov (2020)).	16
4.1	Median and quantiles of various monthly ERA5 variables by year. The data was downloaded from ECMWF (1950-Present) , where detailed information is available.	17

LIST OF FIGURES

v

4.2 Median and quantiles of Pearson correlations between changes in tree genera maps predicted by classification and differences in meteorological conditions.	18
4.3 R ² score of a narrow fully-connected regression neural network using meteorological change maps as predictors for genera change maps derived from tree classification.	19

List of Tables

3.1 Summary of initial hyperparameter search space.	14
---	----

Chapter 1

Data Exploration

1.1 EU-Forest Labels

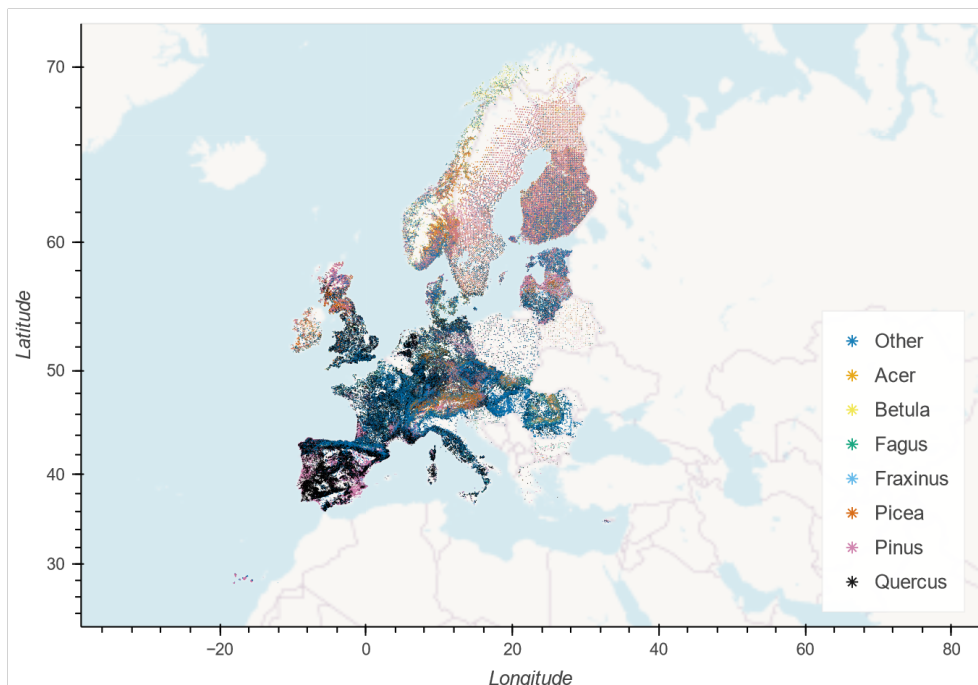


Figure 1.1: Map of the most common tree genera in EU-Forest.

EU-Forest is a dataset containing tree species and genera for nearly 250,000 locations across Europe Mauri et al. (2017). Each plot is $1\text{ km} \times 1\text{ km}$ and may contain multiple tree species and genera. Fig. 1.1 shows the distribution of tree genera in the EU-Forest dataset across 21 European countries. In this figure, the label 'Other' is an umbrella class for 70 tree genera with less than 20,000 occurrences each.

Using the EU-Forest dataset to train a CNN classifier of tree genera with Sentinel-2 data offers several significant advantages. Firstly, the dataset's high spatial resolution enables fine-grained analysis of tree species distribution, which enhances the accuracy of the classifier. Its comprehensive coverage across Europe, including diverse forest types and geographical areas, allows the model to learn from a wide variety of environments and tree genera. The rich occurrence data provides detailed information on tree species, aiding in precise identification and classification.

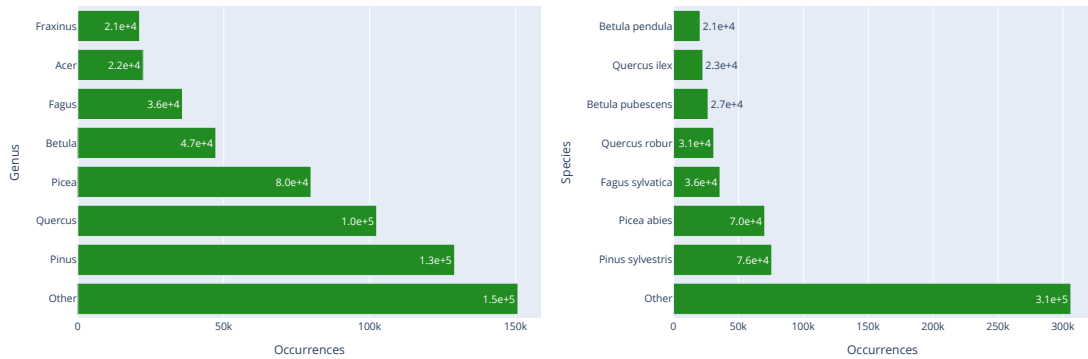


Figure 1.2: Distribution of genera (left) and species (right) in EU-Forest.

Integration with Sentinel-2 satellite data, which provides high-resolution multispectral images, allows for a robust model that leverages both ground-truth data and spectral information. The dataset, being relatively recent, offers a contemporary snapshot of forest conditions, ensuring that the trained model is relevant to current ecological and environmental conditions.

The plots in Fig. 1.2 underscore the prevalence of certain genera and species in European forests, providing valuable insights for training a CNN classifier. The dominance of specific genera and species in the dataset can enhance the classifier's ability to accurately identify and classify tree types when combined with Sentinel-2 data.

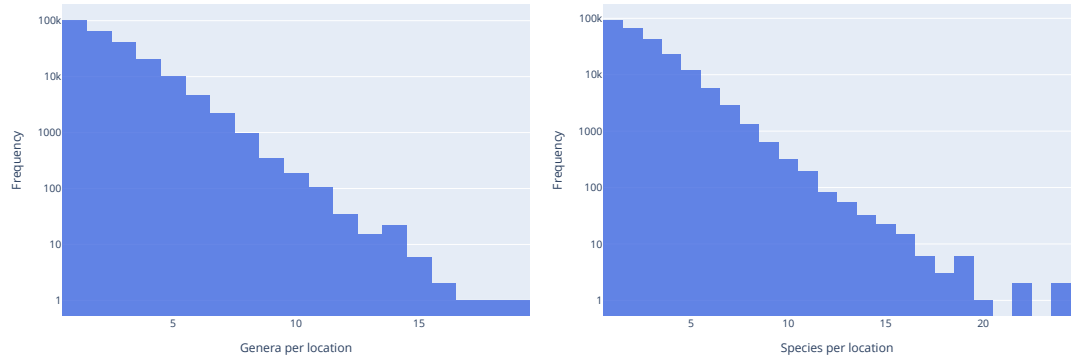


Figure 1.3: Distribution of genera (left) and species (right) per location.

The plots in Fig. 1.3 reveal a common pattern in biodiversity studies: most locations are characterized by a limited number of dominant genera and species, with a smaller number of locations exhibiting higher diversity. This pattern is important for training a CNN classifier, as it indicates that the classifier will often encounter locations with limited genera and species. However, it must also be capable of handling the less common, more diverse locations. The high-frequency, low-diversity areas will likely dominate the training process, influencing the classifier's ability to generalize across different forest types.

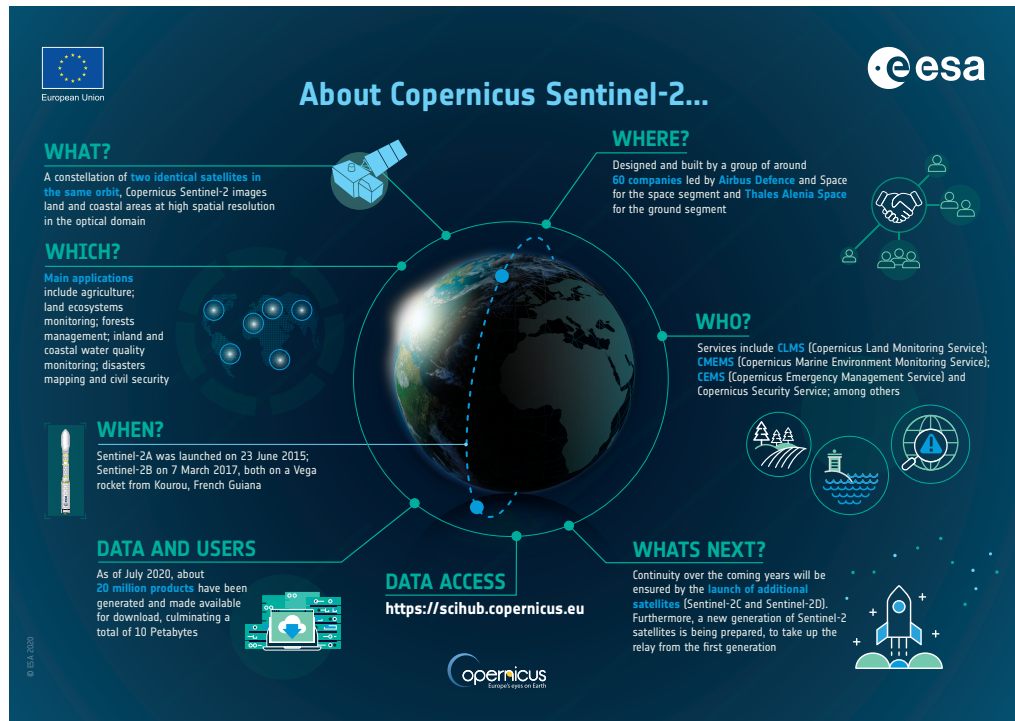


Figure 1.4: Sentinel-2 mission infographic. It highlights important facts and achievements of the mission. Courtesy of [ESA](#).

1.2 Sentinel-2 Features

Using Sentinel-2, Fig. 1.4, specifically the 10-meter and 20-meter resolution bands, for training a CNN classifier of tree genera offers several significant advantages. Sentinel-2 provides high-resolution imagery with these bands capturing detailed spatial information essential for precise classification tasks.

The 10-meter resolution bands include visible red, green, and blue (RGB) wavelengths, as well as near-infrared (NIR) wavelengths, which are essential for assessing vegetation health and differentiating tree genera based on their reflectance properties. The 20-meter resolution bands encompass the red-edge, shortwave infrared (SWIR), and additional near-infrared regions, which enhance the classifier's ability to distinguish between tree genera by capturing subtle variations in spectral signatures. For subsequent analysis, the 20-meter bands were resampled to match the 10-meter resolution.

The multispectral imaging capability of Sentinel-2, with these selected bands, allows for detailed analysis and precise classification of tree genera. Each genus reflects and absorbs light differently across these wavelengths, providing rich data for the classifier to learn from and accurately identify tree types.

Moreover, Sentinel-2 has a frequent revisit time, with satellites passing over the same area every 5 days at the equator. This frequent update cycle is crucial for handling cloud cover, as it increases the likelihood of acquiring cloud-free images, ensuring that the classifier is trained on clear and usable data.

Sentinel-2 also offers extensive geographical coverage, capturing large areas in each image. This comprehensive coverage is essential for training classifiers intended for wide-ranging applications across different forest types and regions, and it supports the development of global models for tree genus classification.

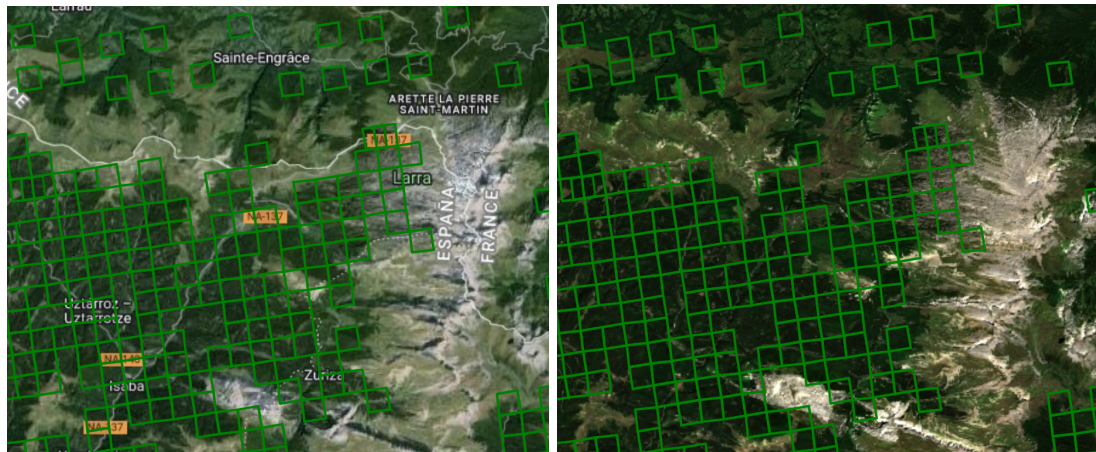


Figure 1.5: Multiple sample locations overlaid on Google Earth (left) and Sentinel-2 (right) images.

Additionally, Sentinel-2 data is freely available through the European Space Agency's Copernicus program and Google Earth Engine. This open access eliminates budget constraints, ensuring high-quality satellite data is accessible for research and operational purposes.



Figure 1.6: Sample location overlaid on Google Earth (left) and Sentinel-2 (right) images.

Figs. 1.5 and 1.6 illustrate the integration of high-resolution geographical context with Sentinel-2 satellite data for detailed environmental analysis. The grid overlay in the images represents areas for data collection and analysis. The left images provide a more detailed geographical context, while the right images show how Sentinel-2 bands B2, B3, and B4 (blue, green, and red respectively) are structured and utilized for spectral analysis.

Figs. 1.7, 1.8, and 1.9 provide a detailed look at the distribution of surface reflectance values and their z-scores for various Sentinel-2 spectral bands, a normalization method which is crucial for many classification tasks using CNNs. These figures use medians taken over the summer months (June, July, and August) between 2017, 2018, and 2019.

Fig. 1.7 shows that the reflectance values for the bands B2, B3, and B4 generally follow a log-normal distribution. The z-scores for these bands peak near zero, demonstrating that the reflectance values have been normalized effectively. This normalization is essential for ensuring that the values from different bands are on the same scale, which is particularly important

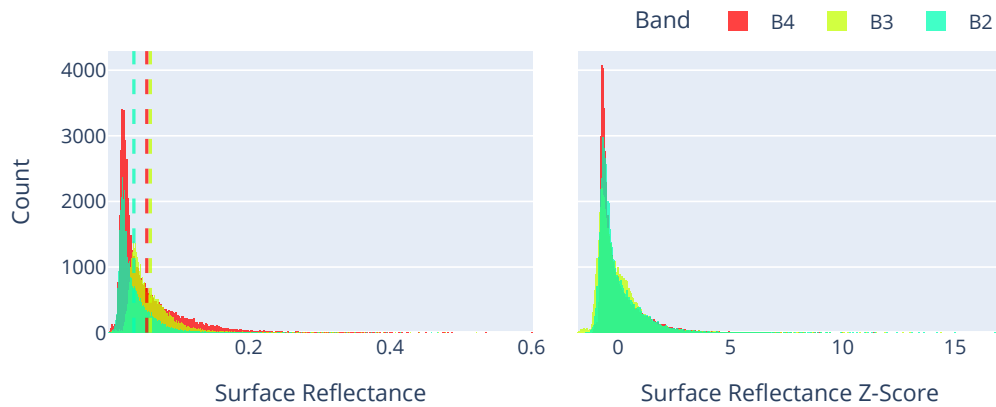


Figure 1.7: Distributions for surface reflectance (left), including a sample means as a dotted line, and z-score normalization (right) for RGB bands.

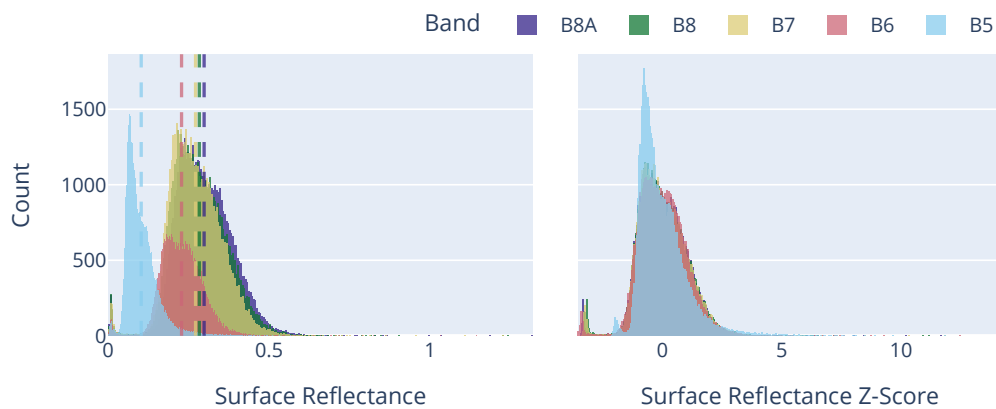


Figure 1.8: Distributions for surface reflectance (left), including a sample means as a dotted line, and z-score normalization (right) for NIR bands.

when using CNN for classification.

Fig. 1.8 presents the distribution for the NIR bands B5, B6, B7, B8, and B8A. The reflectance values for these bands display a central tendency, with a significant number of pixels having values around the mean. The z-score distributions, peaking near zero, indicate successful normalization of the reflectance values. Normalizing the data in this way ensures that the CNN can process and compare these values more effectively, enhancing the model's ability to classify different types of tree genera accurately.

Fig. 1.9 shows histograms for the SWIR bands B11 and B12. The bands display a similar pattern, with the majority of reflectance values clustering on the left of the mean and tailing off to the right of the mean. The z-scores for these bands also peak at zero, confirming that the data has been normalized successfully.

The correlations among different spectral bands of Sentinel-2 data across seasons, as depicted in the correlation matrices in Fig. 1.10, highlight significant patterns that are useful for tree genus classification. All plots show the Pearson's correlation coefficients between various bands, providing insights into how these relationships change with the seasons.

During winter, all bands in NIR and RGB groups show very strong correlations with each other. These high correlations, often close to 1, indicate that the spectral responses of these bands are highly similar during this season. This consistency is likely due to the uniform reflectance properties of vegetation and the ground cover in winter. This strong correlation

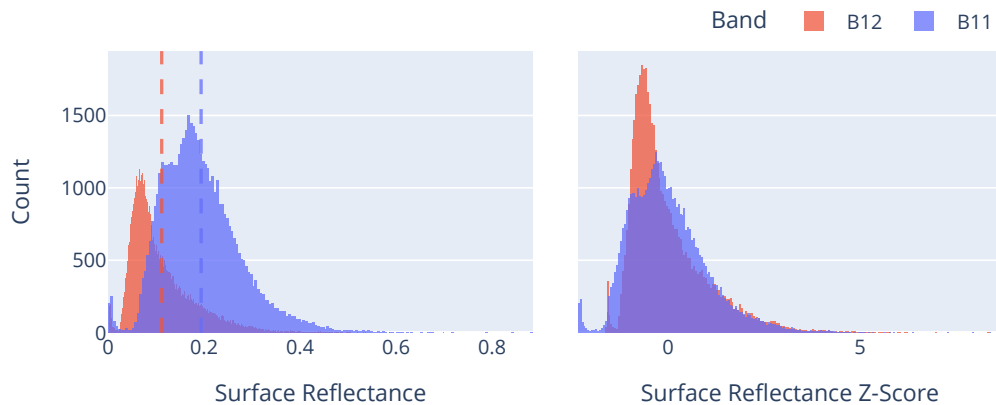


Figure 1.9: Distributions for surface reflectance (left), including a sample means as a dotted line, and z-score normalization (right) for SWIR bands.

is beneficial for tree genus classification as it suggests that the data from these bands can be reliably used to distinguish tree genera based on their reflectance characteristics, or lack thereof, in winter.

In spring, the correlations remain high within the NIR and RGB groups but to a slightly lesser degree compared to winter. The correlation between these two groups starts to decrease, reflecting the changes in vegetation as new growth begins. This seasonal variation provides additional information that can be leveraged to improve the classification models, as the differences in reflectance between the bands become more pronounced.

During summer and autumn, while there are still strong correlations within the NIR and RGB groups, the correlation between these groups is notably lower. This reduced correlation can be attributed to the varying phenological stages of the trees, including differences in leaf development and moisture content. These seasonal changes affect the reflectance properties differently in the NIR and RGB bands. The distinct spectral responses during these seasons offer complementary information that can enhance the classification of tree genera by providing a more diverse set of data points that capture the variability in tree characteristics.

Overall, the varying correlations across seasons underscore the robustness of using Sentinel-2 data for tree genus classification. Normalizing the data using z-scores is crucial as it standardizes the values across different bands, ensuring they are on the same scale. This is particularly important for CNNs, which are sensitive to the relative magnitudes of input data. By bringing the bands to a comparable scale, z-score normalization enhances the model's ability to process and accurately compare the multi-band data, leading to more reliable and precise classification results.

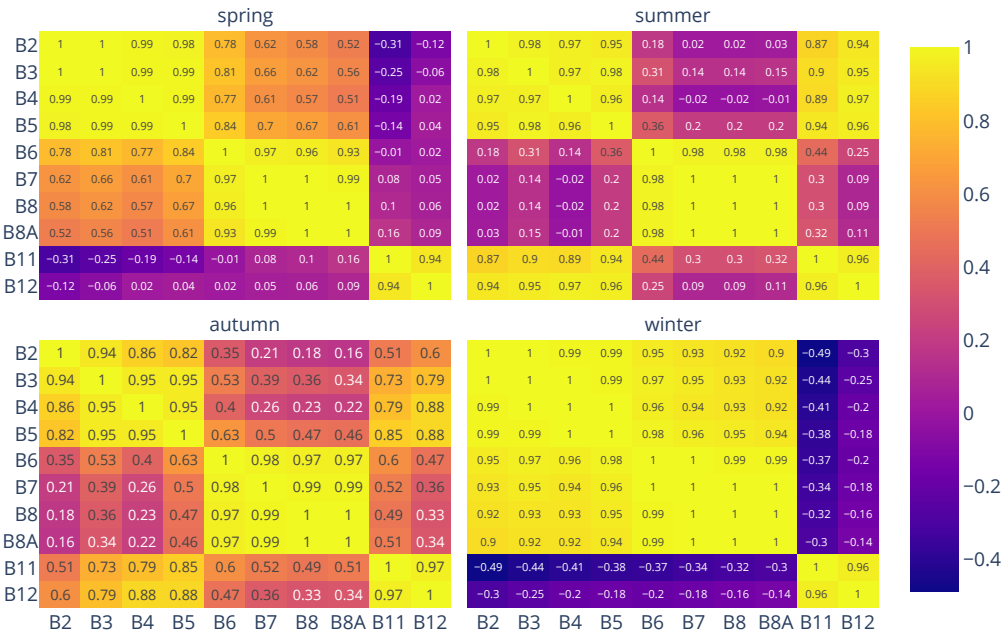


Figure 1.10: Seasonal Sentinel-2 band correlations.

1.3 Copernicus DEM GLO-30

Integrating the Copernicus Global 30 m Digital Elevation Model (DEM) data into the classification model can significantly enhance its performance for tree genus classification. Elevation data provides critical information about the terrain, which influences various ecological factors such as temperature, moisture availability, and soil type. These factors, in turn, affect vegetation types and distribution. The 30 m resolution of the DEM is particularly well-suited for this purpose, as it offers a fine enough scale to capture relevant topographic features while being broad enough to complement the 10 m and 20 m resolutions of Sentinel-2 data. This synergy allows the model to better understand the environmental context of each location, leading to more accurate predictions. For example, certain tree genera may be more prevalent at specific elevation ranges due to their adaptation to particular climatic conditions or soil properties. Therefore, integrating elevation data can help in distinguishing between tree genera that occupy different ecological niches.

Fig. 1.11 presents the distribution of elevation values in meters, as well as the z-scores, which standardize these values. The elevation values range from 0 to around 2500 meters, with most data points clustered below 500 meters. This suggests that the majority of the study area is relatively low-lying. Standardizing elevation values using z-scores is beneficial for integrating elevation data with spectral data, as it ensures that elevation values are on a comparable scale to the reflectance values from Sentinel-2 bands.

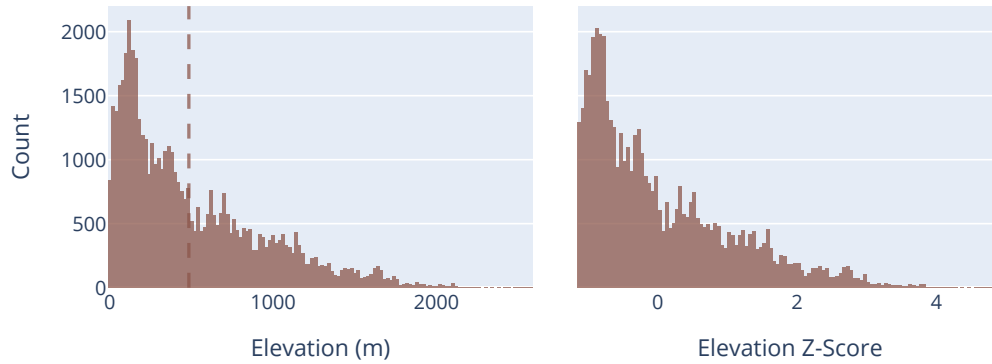


Figure 1.11: Distributions for elevation (left), including a sample means as a dotted line, and z-score normalization (right) for the Copernicus DEM GLO-30 dataset.

1.4 SoilGrids

The SoilGrids dataset (Poggio et al. (2021)) provides global soil information at a spatial resolution of 250 meters and incorporates quantified spatial uncertainty. It includes key soil properties such as organic carbon content, pH, sand, silt, and clay percentages, bulk density, cation exchange capacity, and more. These data are derived from machine learning models trained on extensive soil sample databases and environmental covariates.

Integrating SoilGrids data into the tree genus classification model can significantly enhance its performance. Soil properties profoundly influence vegetation types and distribution, as different tree genera have specific soil requirements and preferences. For instance, soil pH, nutrient content, and texture can determine the suitability of a habitat for particular tree species. By incorporating detailed soil composition data, the model can better understand the environmental context, leading to more accurate predictions of tree genera. This integration helps to account for the ecological niche of each genus, improving the robustness and precision of the classification.

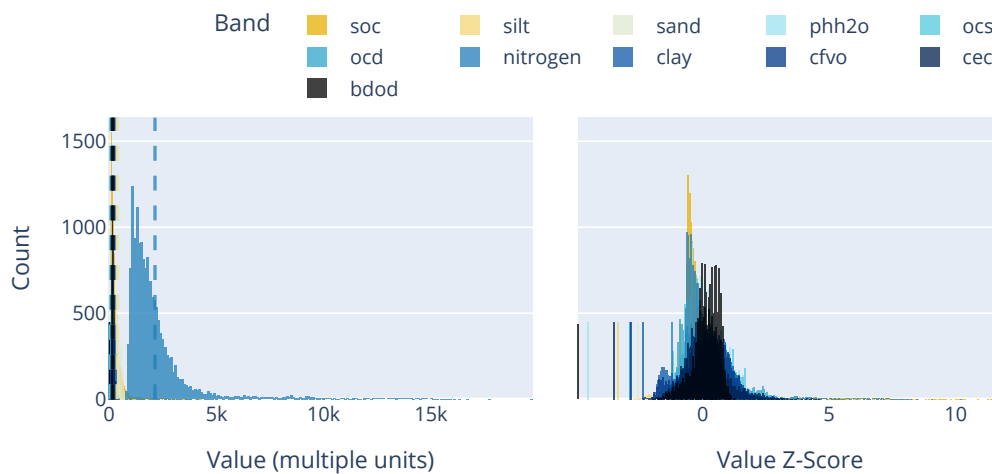


Figure 1.12: Distributions for soil properties (left), including a sample means as a dotted line, and z-score normalization (right) for the SoilGrids dataset.

Fig. 1.12 displays the distribution of various soil properties present in the SoilGrids dataset.

The x-axis represents the value of these properties in multiple units, while the y-axis represents the count of observations. Additionally, the z-score distribution is shown to standardize these values.

The distribution of soil properties varies, reflecting the diversity of soil types across the study area. The z-score distribution standardizes these values, bringing them onto a common scale, which is essential for integrating soil data with spectral and elevation data in the classification model.

In summary, while the integration of high-resolution Sentinel-2 imagery with EU-Forest data, Copernicus DEM elevation information, and SoilGrids soil properties provided a comprehensive dataset, the improvement in model accuracy was marginal. This suggests that, for the task of tree genus classification, the spectral information from Sentinel-2 may be sufficiently robust on its own. However, these additional datasets might still offer value in specific contexts or could enhance model performance in more complex classification tasks or in areas with greater environmental variability.

Chapter 2

Feature Selection

2.1 Sentinel-2 Seasons

Fig. 2.1 shows the performance of the CNN model across different seasons, with metrics including recall, precision, weighted f1-score, precision-recall curve area under the curve (PRC), and receiver operating characteristic area under the curve (AUC). Filled boxes indicate the combination of seasons used to train and validate the model. Blue boxes indicate a combination of 3D CNN and fully-connected layers and the orange box indicates the use of a similar model but with the introduction Long Short-Term Memory (LSTM) alongside 3D convolutions and fully-connected layers.

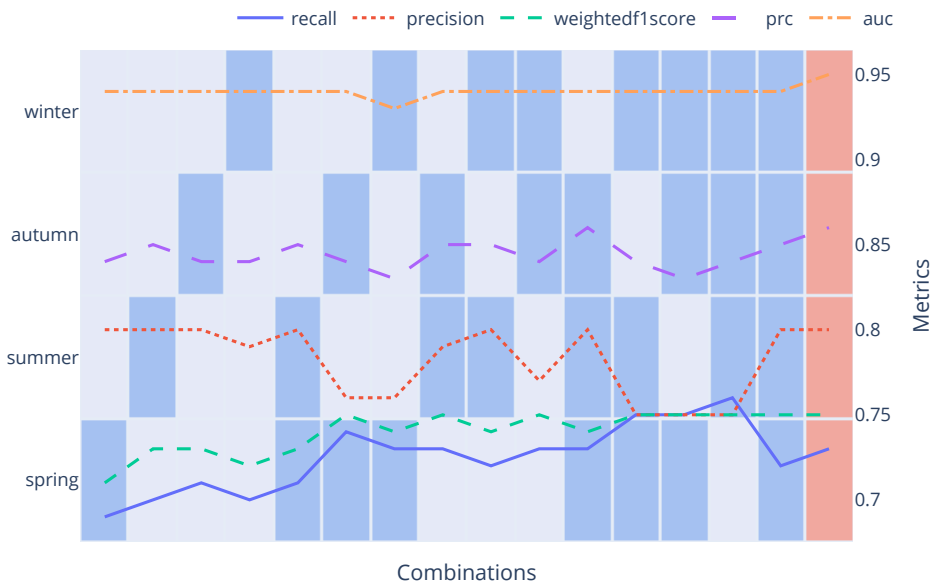


Figure 2.1: Seasonal Sentinel-2 analysis for all season combinations using a 3D CNN.

3D convolutions were selected for this model due to their suitability for this problem as they can effectively capture the spatial and spectral dependencies in the multi-temporal Sentinel-2 data. By considering the additional temporal dimension, 3D convolutions can leverage seasonal variations and changes in vegetation phenology, which are crucial for accurate tree genus classification.

LSTM was introduced to the model alongside 2D convolutions because they process the spatial structure of the Sentinel-2 images through convolution operations while simultaneously capturing temporal sequences. This dual capability allows the model to learn intricate spatial patterns within each image and understand how these patterns evolve over time.

The selected metrics used to create Fig. 2.1 are well-suited for handling class imbalance in the seasonal analysis of the CNN model. Recall ensures the model captures as many instances of the minority classes as possible, which is critical when dealing with imbalanced datasets. Precision assesses the accuracy of the model's positive predictions, reducing the impact of false positives. The weighted f1-score balances precision and recall, accounting for class imbalance by considering the support of each class. PRC focuses on the trade-off between precision and recall, highlighting the model's performance on minority classes. Lastly, AUC measures overall model performance across all thresholds, providing a comprehensive view of its ability to distinguish between classes.

For individual seasons, the model performs best in summer and autumn overall across the metrics. This suggests that the CNN model is more effective at classifying tree genera during these times, likely due to clearer and more distinct spectral signatures in the data collected during summer and autumn. The lower performance in spring and winter might be attributed to less distinct spectral signatures or more challenging environmental conditions, such as cloud cover and snow, which can affect data quality.

Based on the weighted f1-scores shown in Fig. 2.1, adding more seasons does not seem to offer significant benefits. For instance, some two-season combinations, such as summer and autumn, performed on par with the more complex four-season models. Additionally, single-season models were only a few percentage points below the top-performing models.

Based on these results, further analysis focused solely on summer seasons. This approach benefits from faster model training and reduced storage requirements, as adding an extra season nearly doubles the storage needs, a challenge that intensifies with the extension of the analysis over additional years. Despite these adjustments, a complete Sentinel-2 dataset for a single season still requires nearly 200 GB, or approximately 1 MB per location.

2.2 Sentinel-2 Bands

In addition to the seasonal analysis in Section 2.1, another analysis was conducted to identify the most effective band combinations. Due to the large number of possible combinations, a direct analysis was impractical. Instead, Sentinel-2 bands were divided into three groups based on summer correlation groupings shown in Fig. 1.10: B2, B3, B4, and B5; B6, B7, B8, and B8A; and B11 and B12.

The resulting analysis, shown in Fig. 2.2, indicates that NIR and SWIR bands perform slightly better overall. Based on these results, another group was selected: B2, B3, B6, B8, and B11. These bands represented the best combinations that resulted in a practical analysis within the available timeframe.

Fig. 2.3 shows that most selected combinations performed relatively well, as indicated by their proximity to the weighted f1-score for all bands. Based on these results, the most reasonable choices appear to be B3, B8, and B11, or the same but with B6 in addition. As the B6 combination displays better recall, precision, and weighted f1-score, as well as taking a fraction of storage compared to 10 m bands due to being 20 m. For the 250,000 samples, this combination should take roughly 50 GB of storage. As such, the combination B3, B6, B8, and B11, was used for the remainder of this study.



Figure 2.2: Sentinel-2 analysis for all combinations within three band groups using a CNN. The horizontal black line represents the weighted f1-score for all bands.

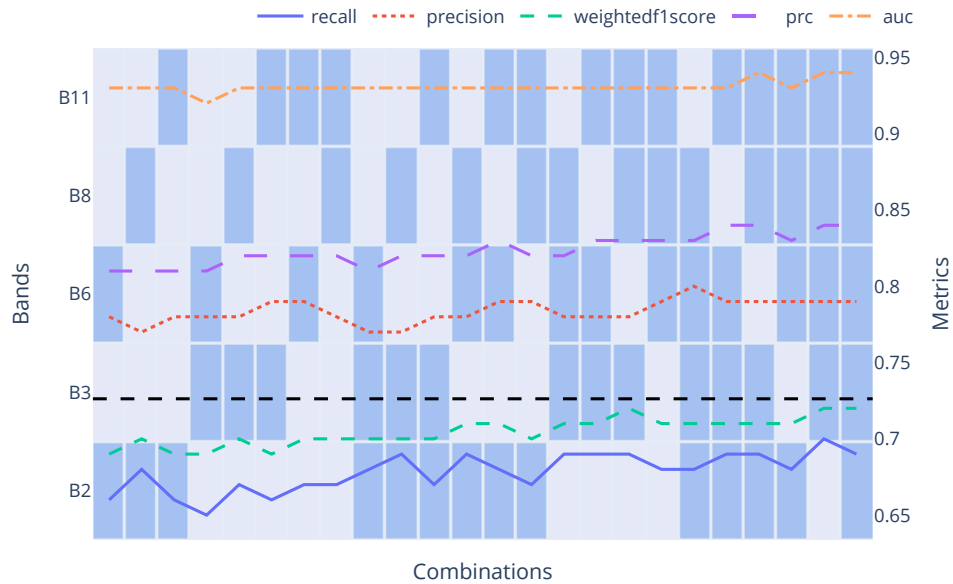


Figure 2.3: Sentinel-2 analysis for selected combinations between each of the three groups using a CNN. The horizontal black line represents the weighted f1-score for all bands.

2.3 Soil and Elevation

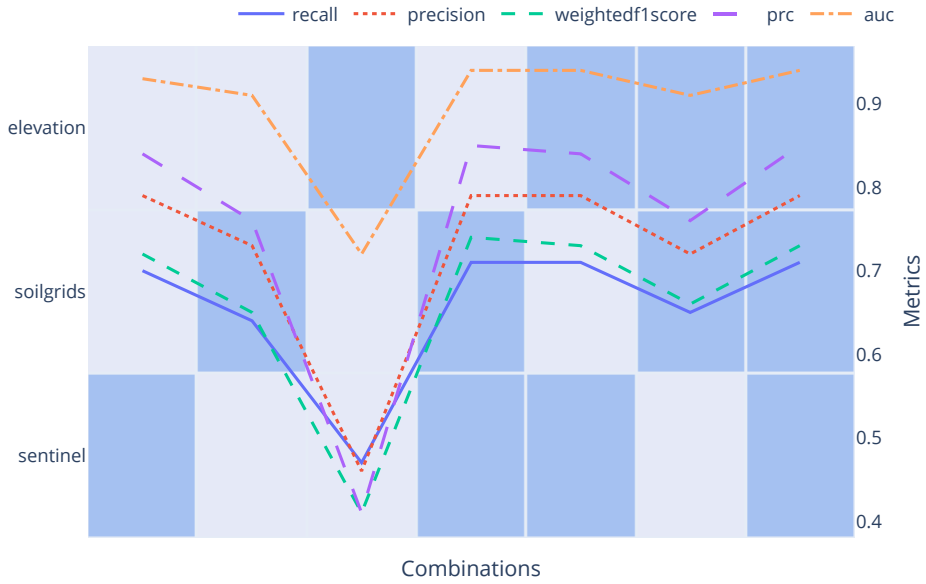


Figure 2.4: Analysis of SoilGrids and elevation data integration.

Fig. 2.4 demonstrates the performance metrics for different combinations of Sentinel-2, SoilGrids, and elevation data in tree genus classification. Sentinel-2 data alone provides a solid baseline, attributed to its high resolution and rich spectral information. When considering SoilGrids data alone, the metrics are lower than those for Sentinel-2, reflecting the coarse resolution and potentially limited predictive power for this specific task. Similarly, elevation data alone shows lower performance metrics, indicating that while elevation is a relevant feature, it does not provide sufficient information by itself for accurate classification of tree genera. The combined use of these datasets shows marginal improvements, suggesting that while additional data may contribute some value, Sentinel-2's high-resolution spectral data is the most significant factor in the model's performance.

Given that Sentinel-2 data alone provides strong results, further enhancements and optimizations were solely focused on this dataset.

Chapter 3

Neural Network Configuration

3.1 Hyperparameter Optimization

Table 3.1 provides a summary of the search space for the initial hyperparameter tuning process. These parameters are critical as they influence the model's learning process, generalization ability, and susceptibility to issues such as overfitting or bias. The chosen values in the search space represent a balance between exploring a wide range of options and focusing on promising areas based on prior knowledge or domain-specific considerations.

In the most successful trial, the model utilized training data from the medians of 2017, 2018, and 2019, applied L1L2 kernel regularization, used a spatial dropout rate of 0.5, and employed Leaky ReLU activation. The pool size was set to 4, dropout to 0.1, and bias initialization was disabled. The learning rate was 0.01, and the loss function was binary crossentropy, resulting in a score of 0.69.

While some of the initial trial's hyperparameters do not show significant overall improvement, some parameters do stand out. This is illustrated in Fig. 3.1, particularly regarding training years, kernel regularization, activation function, and learning rate.

Table 3.1: Summary of initial hyperparameter search space.

name	values
class_weight	[true, false]
training_years	['2017_2018_2019', '2017']
kernel_regularizer	['l1l2', 'l1', 'l2']
spatial_dropout	[0.3, 0.1, 0.5]
activation	['leaky_relu', 'relu']
pool_size	[4, 2]
dropout	[0.3, 0.1, 0.5]
bias_initializer	[true, false]
learning_rate	[0.001, 0.0001, 0.01]
loss_function	['binary_focal_crossentropy', 'binary_crossentropy']

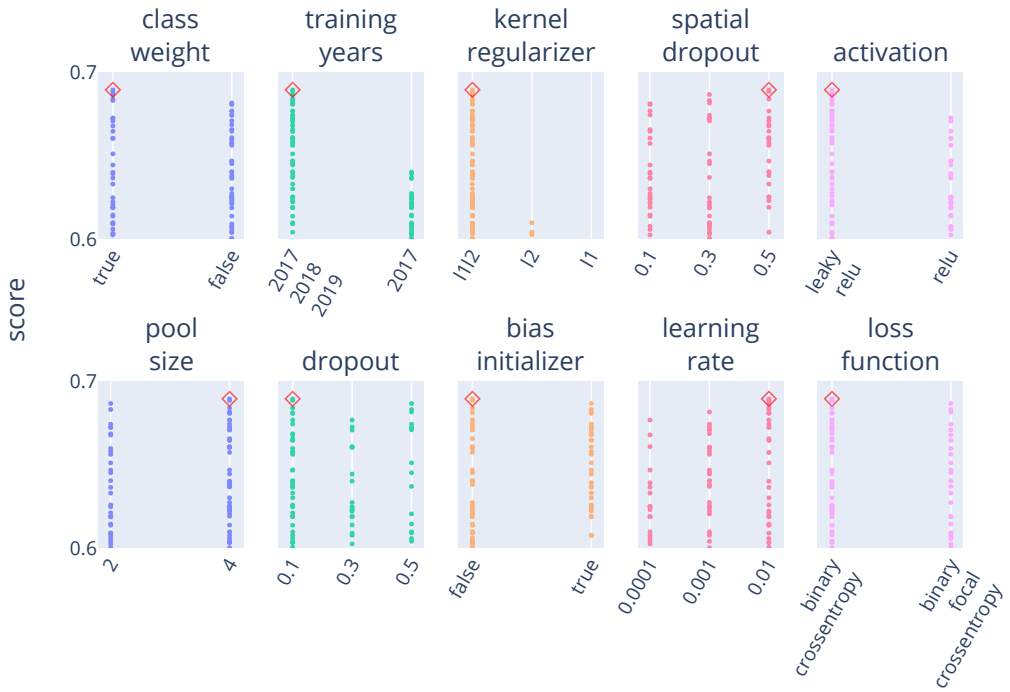


Figure 3.1: The top f2-scores for the initial hyperparameter tuning process are highlighted, with the best score marked by a diamond shape.

3.2 Model Architecture

Fig. 3.2 illustrates the detailed architecture of the deep learning model, highlighting the flow of data through its various layers. The model starts with input layers, which include upsampling layers to handle inputs with different dimensions. This ensures that all input sources are properly aligned for processing within the model. The network then progresses through multiple convolutional layers, with filter sizes generally increasing as the layers deepen. Batch normalization and dropout layers are strategically placed to regularize the model and prevent overfitting.

The architecture incorporates residual connections for maintaining gradient flow during backpropagation. These connections enable the network to be deep without suffering from issues like vanishing gradients, as highlighted in He et al. (2015). As the network advances, spatial dimensions are reduced through pooling and striding operations, leading to a flattening layer that prepares the data for the fully connected (dense) layers. These dense layers further reduce the dimensionality, eventually outputting a 7-dimensional vector corresponding to the classification into 7 different tree genera, aligning with the model's goal of predicting tree types.

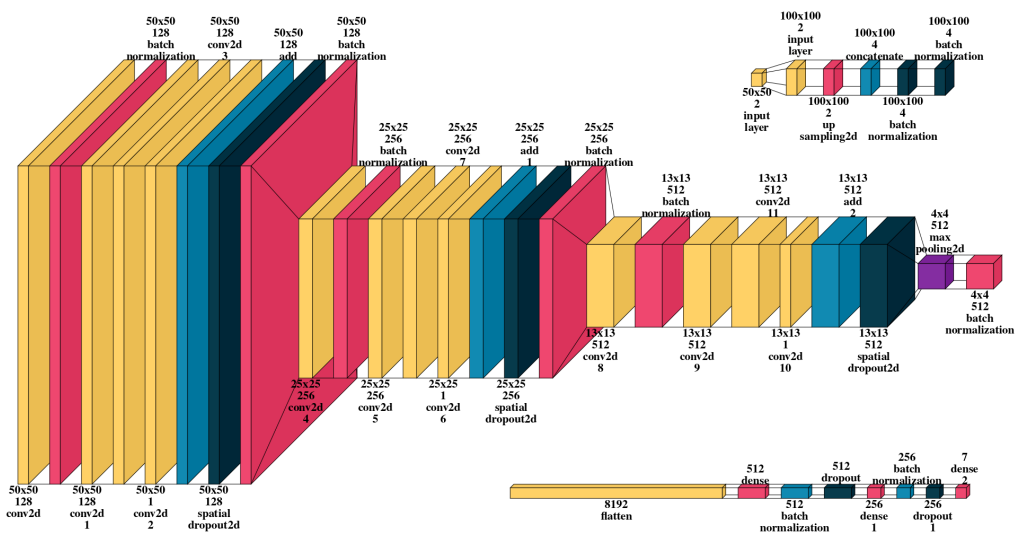


Figure 3.2: The model's layered architecture is depicted. The top-right shows the input layers, the middle section displays the convolutional layers, and the bottom-right illustrates the fully-connected layers. The layered views were generated using VisualKeras (Gavrikov (2020)).

Chapter 4

Climate Analysis

4.1 ECMWF Reanalysis v5 Dataset

The ECMWF Reanalysis v5 (ERA5) dataset (Hersbach et al. (2020)) was selected for correlating with tree genus classification due to its extensive and high-resolution climate data, which includes variables such as temperature, precipitation, and soil moisture. This dataset offers detailed historical weather information, capturing both spatial and temporal variations essential for understanding the environmental conditions that impact tree growth and distribution. By leveraging ERA5 data, this study aimed to explore how different climate factors might influence the abundance of various tree genera.

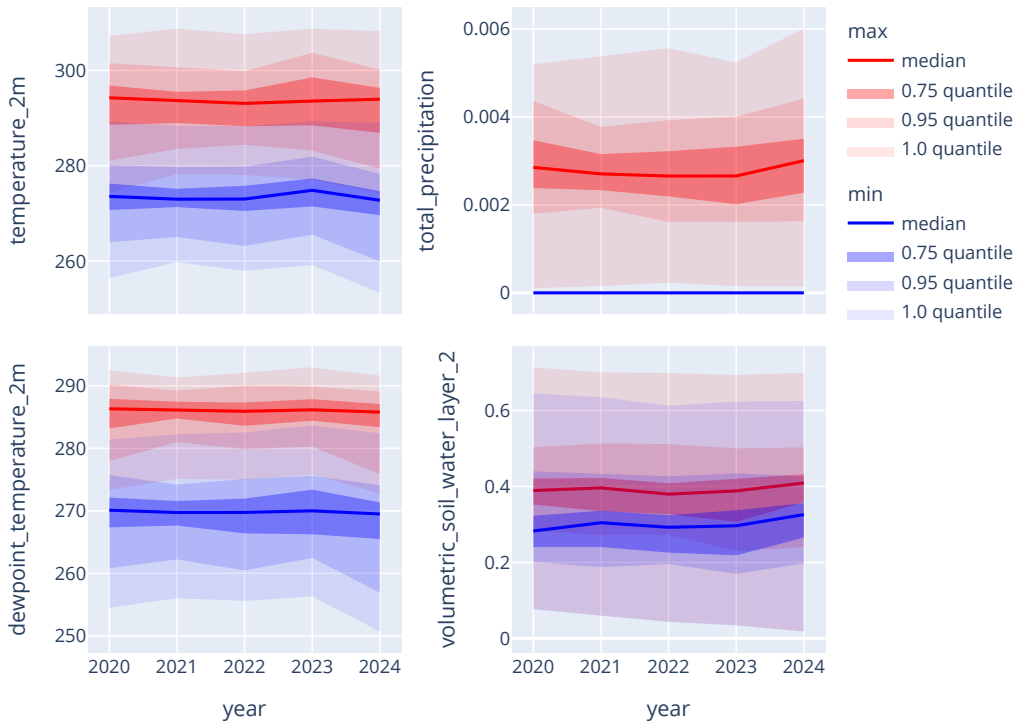


Figure 4.1: Median and quantiles of various monthly ERA5 variables by year. The data was downloaded from ECMWF (1950-Present), where detailed information is available.

As the ERA5 dataset contains numerous meteorological variables, a selection was made based on domain knowledge and studies such as Toledo et al. (2011). Fig. 4.1 summarizes this selection, showing the median and quantiles for the aggregated dataset across all study locations. The figure illustrates the significant variability within Europe, with the top-left plot indicating a difference of approximately 50 K between the 1.0 quantile of minimum and maximum temperature measurements.

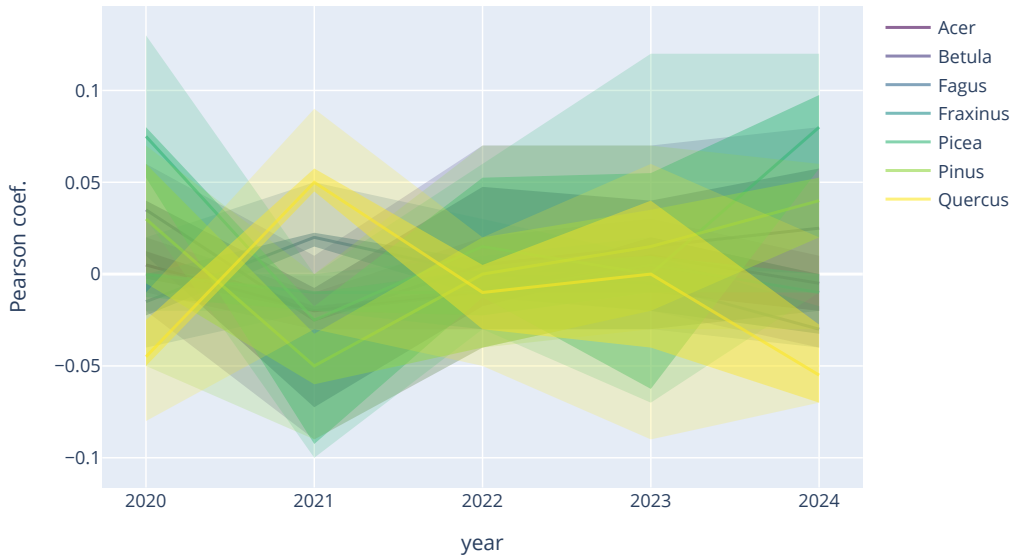


Figure 4.2: Median and quantiles of Pearson correlations between changes in tree genera maps predicted by classification and differences in meteorological conditions.

The representative medians of the variables shown in Fig. 4.1 were calculated for the years 2010 to 2017. The differences between these medians and those for each individual year from 2020 to 2024 were analyzed and correlated with the discrepancies between classification predictions and actual values. These results are summarized in Fig. 4.2. This figure suggests that, over a short-term period of 5 years, the 7 most prominent European tree genera were not significantly affected by climate change. However, this does not account for potential long-term impacts, where even small changes could have substantial effects on ecological dynamics. Additionally, the analysis is limited to Europe, which may experience less pronounced climate changes compared to other regions that are more severely affected. Furthermore, the study does not consider less frequent tree genera, which might be more sensitive to climate change and could exhibit different patterns of response.

To further verify the results shown in Fig. 4.2, a narrow fully-connected regression neural network was developed. This network used the change map of meteorological variables as predictors to estimate changes in the tree genera maps.

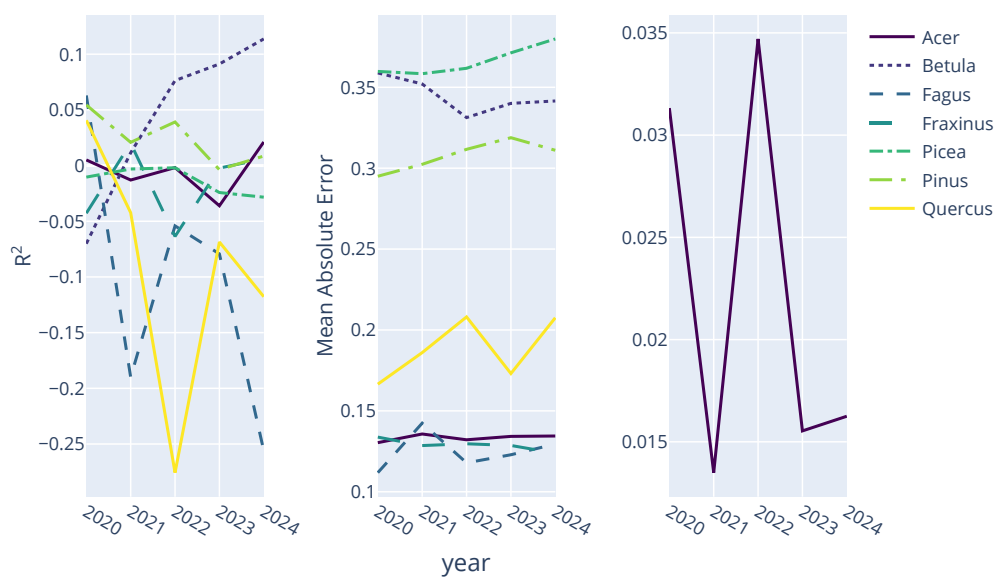


Figure 4.3: R^2 score of a narrow fully-connected regression neural network using meteorological change maps as predictors for genera change maps derived from tree classification.

References

- ECMWF (1950-Present), 'ERA5-Land Monthly Aggregated ECMWF Climate Reanalysis', https://developers.google.com/earth-engine/datasets/catalog/ECMWF_ERA5_LAND_MONTHLY_AGGR.
- Gavrikov, P. (2020), 'visualkeras', <https://github.com/paulgavrikov/visualkeras>.
- He, K., Zhang, X., Ren, S. and Sun, J. (2015), 'Deep residual learning for image recognition'.
- Hersbach, H., Bell, B., Berrisford, P., Hirahara, S., Horányi, A., Muñoz-Sabater, J., Nicolas, J., Peubey, C., Radu, R., Schepers, D., Simmons, A., Soci, C., Abdalla, S., Abellán, X., Balsamo, G., Bechtold, P., Biavati, G., Bidlot, J., Bonavita, M., De Chiara, G., Dahlgren, P., Dee, D., Diamantakis, M., Dragani, R., Flemming, J., Forbes, R., Fuentes, M., Geer, A., Haimberger, L., Healy, S., Hogan, R. J., Hólm, E., Janisková, M., Keeley, S., Laloyaux, P., Lopez, P., Lupu, C., Radnoti, G., de Rosnay, P., Rozum, I., Vamborg, F., Villaume, S. and Thépaut, J.-N. (2020), 'The ERA5 global reanalysis', *Quarterly Journal of the Royal Meteorological Society* **146**(730), 1999–2049.
- Mauri, A., Strona, G. and San-Miguel-Ayanz, J. (2017), 'EU-Forest, a high-resolution tree occurrence dataset for Europe', *Scientific Data* **4**(1), 160123.
- Poggio, L., de Sousa, L. M., Batjes, N. H., Heuvelink, G. B. M., Kempen, B., Ribeiro, E. and Rossiter, D. (2021), 'SoilGrids 2.0: producing soil information for the globe with quantified spatial uncertainty', *SOIL* **7**(1), 217–240.
- Toledo, M., Poorter, L., Peña-Claros, M., Alarcón, A., Balcázar, J., Leaño, C., Licona, J. C., Llanque, O., Vroomans, V., Zuidema, P. and Bongers, F. (2011), 'Climate is a stronger driver of tree and forest growth rates than soil and disturbance', *Journal of Ecology* **99**(1), 254–264.